Hindawi
Advances in Materials Science and Engineering
Volume 2020, Article ID 6142945, 13 pages
https://doi.org/10.1155/2020/6142945

Research Article

Compression and Shear Fracture Analysis of Boundary Cracks Containing Water in Rock

Zhensheng Yang,[1,2] Fulin Li ,[1,2] and Tianran Ma[2]

[1]*State Key Laboratory for Geomechanics and Deep Underground Engineering, China University of Mining and Technology, Xuzhou, Jiangsu 221116, China*
[2]*School of Mechanics and Civil Engineering, China University of Mining and Technology, Xuzhou, Jiangsu 221116, China*

Correspondence should be addressed to Fulin Li; lifulin@cumt.edu.cn

Received 30 April 2020; Revised 11 June 2020; Accepted 16 June 2020; Published 20 July 2020

Academic Editor: Pasquale Gallo

Copyright © 2020 Zhensheng Yang et al. This is an open access article distributed under the Creative Commons Attribution License, which permits unrestricted use, distribution, and reproduction in any medium, provided the original work is properly cited.

In order to conserve the water resource during underground mining, the fracture and mechanical properties of rock are important for the stability of water-resisting layers, especially for the fracture behavior of boundary cracks containing water in rock. Considering the swelling of rock under water environment and the influence of water on rock, the stress intensity factors of modes I and II are derived for boundary cracks in rock under compressive and shear stresses. The cracks are divided into the closed and open states. The effects of the crack inclination angle, friction coefficient between crack surfaces, and initial crack length on stress intensity factors are also taken into account. The stress intensity factors for closed and open boundary cracks are verified by numerical and physical experiments, respectively, and the deviation of the results is within 5%. It is shown that pore pressure has different effects on the relationship between stress intensity factor and friction coefficient under different lateral pressures. The effect of water on crack propagation is mainly due to the deterioration of the fracture toughness of the rock. It is found that the critical coefficient λ_c is a key parameter to determine whether the boundary crack propagates in rock under compression-shear stress. Further studies should be performed to apply the present fracture theory to rock mass or water-resisting layers.

1. Introduction

Water has a significant effect on the fracture and mechanical properties of rock materials [1–4]. And a host of geological hazards and engineering disasters are closely related to water, such as landslides, karst collapse, fault activation, water inrush in mine, instability of water-resisting layer, and so on [5, 6]. As coal mining moves westward in China, it has significant importance to conserve the water resource in the arid and semiarid areas of Northwest China. Due to the disturbance of underground mining or construction, the initial cracks are produced in the water-resisting strata, which are mainly composed of sandstone, shale, and clay. The water intrusion becomes an important factor that leads to the crack propagation until ultimately penetrating the whole rock stratum. In the condition of water environment, the geometric parameters of cracks and the water content will have a significant impact on the fracture and mechanical properties of rock. Yang et al. [7] performed a set of conventional triaxial compression tests on dry and brine-saturated sandstone specimens containing two preexisting three-dimensional flaws. It was shown that the peak strength and crack damage stress of the sandstone specimens increased as the flaw angle increased. Zuo et al. [8] conducted three-point bending tests on semicircular bend (SCB) sandstone specimens; the results showed that the peak load of the specimen exponentially increases with the increase of crack inclination angle. Guha Roy et al. [9] investigated the mechanical and fracture properties of sedimentary rocks, which were three types of sandstones and one type of shale saturated in water for different periods of time. The degree of saturation has significant effect on both the strength and fracture properties of sedimentary rocks. Yao [10] developed a 3D pore pressure cohesive zone model to predict hydraulic

fracturing with different rock properties under fluid injection. Huang and Liu [11] studied the influence of shale bedding on the propagation of cracks containing water and summarized the propagation law of cracks for hydraulic fracture under true triaxial stresses when they meet the bedding plane.

Fracture toughness is a rock's property in the presence of a preexisting flaw, which governs the critical stress at which a crack in rock becomes unstable and propagates. The semicircular bend (SCB) specimens have been widely used for fracture toughness determination of rocks [8, 12–18]. Lim et al. [13, 14] proved that the water saturation is a dominant factor affecting the fracture toughness of soft rocks and the fracture toughness increases with strain rate. Furthermore, Mahanta et al. [15] indicated that the fracture toughness and the energy release rate for mode I, mode II, and mixed mode are a function of strain rate. Kataoka et al. [16] investigated the influence of water vapor pressure in the surrounding environment on mode I fracture toughness of rocks. Combining semicircular bend specimens with acoustic emission monitoring, Zhou et al. [17] found that the fracture toughness and crack growth rate of sandstone would decrease with the increase of water content. For a clay-bearing sandstone, the fracture toughness decreases as relative humidity increases depending on the orientation of the microcracking and the toughness anisotropy appears during humidification [18]. Moreover, Hua et al. [19] used centrally cracked Brazilian disk specimens to study the effect of cyclic wetting and drying on the fracture toughness and crack propagation of rock. Using nanoindentation, Gupta et al. [20] measured both tensile and shear dominated fracture toughness in shales, where crack length method and energy method are suitable to mode I (tensile) and mode II (shear) fracture toughness, respectively.

In recent years, several criteria were presented for the fracture of rock, which determines whether a crack propagates or nucleates. Savitski and Detournay [21] obtained the asymptotic solution of the propagation criterion of the elliptical center crack containing fluid in the low permeable rock by analytical method. It is considered that three crack propagation regimes are identified: viscosity and fracture toughness dominated, as well as mixed regimes. The relationship between initial fracture geometry, rock compressive strength, and fracture toughness is explored from experiment and theory, which provides theoretical guidance for engineering practice [22, 23]. Dong et al. [24] developed a unified interfacial crack initiation criterion expressed by the stress intensity factors, by performing three-point bending and four-point shear tests on the composite rock-concrete specimens. Sih [25] presented the K_I-K_{II} curve that governs the mixed mode fracture of cracks under remote compression. Then, according to the special stress condition of underground rock mass, Zhou [26] proposed the fracture criterion of compression-shear crack of I-II mixed mode by the unilateral crack test. Based on the basic energy release rate criterion, Shen and Stephansson [27] put forward an F criterion which accords with the rock compression-shear fracture model. In order to improve the prediction accuracy of mode II stress intensity factor, Ayatollahi and Stananinia [28] proposed the maximum tangential stress criterion, which takes into account the first three terms of William's series expansion for elastic stresses at crack tip. Also, Zheng and Luo [29] deduced the criterion expression of compression-shear crack theoretically in combination with different failure criteria.

However, the current research mainly focused on the mechanical and fracture properties of central crack in rock under compression and shear state during underground mining or construction. The fracture behavior of boundary cracks in the compression-shear state has been rarely investigated in the literature, especially under the water action after the initial cracks in rock are produced due to the influence of mining or construction. And the crack opening state in rock is usually not considered strictly. Therefore, the mechanical and fracture analysis of boundary cracks containing water in rock is carried out in the present study. The expressions of modes I and II stress intensity factors of the boundary cracks in the compression-shear stress state are obtained for both open and closed cracks. Subsequently, the corresponding stress intensity factors are verified by physical and numerical experiments, respectively. It provides a theoretical basis for estimating the instability law of boundary cracks in rock by compression-shear coefficient, which is a key parameter of rock.

2. Stress Intensity Factors for Cracks Containing Water

Under the disturbance of underground engineering such as mining, the occurrence of cracks in underground aquifer strata can be divided into the upward and downward cracks. The downward cracks are generally in the state of compression-shear stress due to the existence of in situ stress and the upper water pressure. The crack propagation can be described as the I-II compression-shear combined type. And the fracture criterion for the compression-shear rock crack can be formulated as follows [25, 26, 29]:

$$\lambda K_I + |K_{II}| = K_{IIc}, \tag{1}$$

where K_I and K_{II} are the stress intensity factors of modes I and II, respectively. K_{IIc} is the mode II fracture toughness of rock and λ is the compression-shear coefficient of rock. Considering the crack opening state, it can be divided into the closed and open cracks. The criterion for a crack to be open or closed was derived by David and Zimmerman [30]. The two-dimensional model is shown in Figure 1.

2.1. Stress Intensity Factors for Closed Cracks. Due to the influence of groundwater in the upper part of the crack, the mechanical action and the swelling effect of rock within water mainly affect the stress intensity factors at the crack tip. The mechanical action mainly includes the far-field stress, the pore pressure, and the friction between crack surfaces. Therefore, the stress intensity factor can be obtained by superimposing those produced by these two factors, respectively. For the closed cracks, the stress intensity factor is expressed as

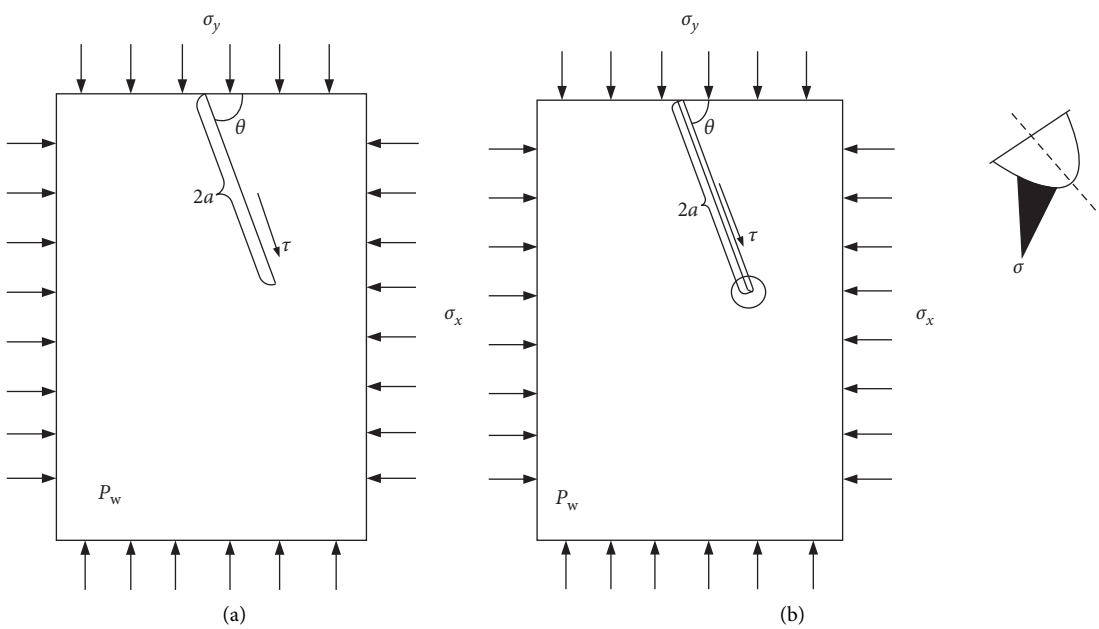

Figure 1: Schematic diagram of simplified mechanical model for boundary cracks in compression-shear state. (a) Closed crack. (b) Open crack.

$$K_{\mathrm{I}}^{\mathrm{b}} = K_{\mathrm{I}}^{\mathrm{p}} + K_{\mathrm{I}}^{\mathrm{h}},$$
$$K_{\mathrm{II}}^{\mathrm{b}} = K_{\mathrm{II}}^{\mathrm{p}} + K_{\mathrm{II}}^{\mathrm{h}}, \tag{2}$$

where $K_{\mathrm{I}}^{\mathrm{b}}$ and $K_{\mathrm{II}}^{\mathrm{b}}$ are the stress intensity factors of modes I and II closed cracks, respectively. $K_{\mathrm{I}}^{\mathrm{p}}$ and $K_{\mathrm{II}}^{\mathrm{p}}$ are the modes I and II stress intensity factors caused by the mechanical action, and $K_{\mathrm{I}}^{\mathrm{h}}$ and $K_{\mathrm{II}}^{\mathrm{h}}$ are the modes I and II stress intensity factors caused by the swelling effect of rock within water.

For the stress intensity factors caused by the mechanical action, the basic form of the modes I and II closed cracks is described as follows, which is according to the stress intensity factor of the boundary crack in a semi-infinite plate obtained by using the theories of complex variable function and rational mapping function [31]:

$$\begin{cases} K_{\mathrm{I}}^{\mathrm{p}} = -\sigma_n \sqrt{2\pi a}, \\ K_{\mathrm{II}}^{\mathrm{p}} = -\tau_p \sqrt{2\pi a}, \end{cases} \tag{3}$$

where σ_n and τ_p are the stresses of crack tip in the normal and tangential directions, respectively. $2a$ is the length of crack. The negative sign indicates that the mode I stress intensity factor hinders the tensile fracture of the crack under compression-shear condition.

The analysis of crack growth depends mainly on the stress field at the crack tip. The magnitude of normal stress σ_n and tangential stress τ at the boundary crack tip can be determined as

$$\sigma_n = \sigma_y \cos^2\theta + \sigma_x \sin^2\theta, \tag{4}$$

$$\tau = \left(\sigma_y - \sigma_x\right)\cos\theta\sin\theta. \tag{5}$$

Taking into account that the pore pressure caused by the existence of groundwater above the rock layer and the friction effect caused by rough surface when the closed crack surface is dislocated relatively, equations (4) and (5) change to

$$\sigma_n = \sigma_x \sin^2\theta + \sigma_y \cos^2\theta - P_{\mathrm{w}}, \tag{6}$$

$$\tau_p = \tau - f\sigma_n = \left(\sigma_y - \sigma_x\right)\cos\theta\sin\theta - f\left(\sigma_x \sin^2\theta + \sigma_y \cos^2\theta\right) + fP_{\mathrm{w}}, \tag{7}$$

where f is the friction coefficient of crack surface. It is found that $f \in [0.18, 0.8]$, which was measured by using the electronic universal testing machine CSS-55000 and the self-made test box. P_{w} is the pore pressure of rocks.

Thus, equations (6) and (7) can be substituted for equation (3). The expression of stress intensity factor for closed crack without considering the swelling is as follows:

$$K_{\mathrm{I}}^{\mathrm{p}} = \left(P_{\mathrm{w}} - \sigma_x \sin^2\theta - \sigma_y \cos^2\theta\right)\sqrt{2\pi a}, \tag{8}$$

$$K_{\mathrm{II}}^{\mathrm{p}} = -\left[\left(\sigma_y - \sigma_x\right)\cos\theta\sin\theta - f\left(\sigma_x \sin^2\theta + \sigma_y \cos^2\theta\right) + fP_{\mathrm{w}}\right]\sqrt{2\pi a}. \tag{9}$$

When considering the swelling effect of water on rock immersion, Liang et al. [32] performed experiments and theoretical analyses to indicate that the hydration swelling stress mainly affects the stress intensity factor of mode I crack. At this moment, $K_{\mathrm{II}}^{\mathrm{h}}$ is equal to 0. Then, the stress intensity factor of rock produced by the swelling is obtained as

$$K_{\mathrm{I}}^{\mathrm{h}} = 2P_{\mathrm{h}}\sqrt{\frac{2a}{\pi}}\arcsin\left(\frac{b}{2a}\right), \tag{10}$$

where P_{h} is the hydration stress produced by the swelling, which should be measured by experiments on rocks. b is the length of the hydration stress applied to the crack surface.

Finally, the mode I stress intensity factor of closed crack containing water can be expressed as

$$K_{\mathrm{I}}^{\mathrm{b}} = \left(P_{\mathrm{w}} - \sigma_x \sin^2\theta - \sigma_y \cos^2\theta\right)\sqrt{2\pi a} + 2P_{\mathrm{h}}\sqrt{\frac{2a}{\pi}}\arcsin\left(\frac{b}{2a}\right). \tag{11}$$

At the same time, the compression-shear fracture criterion for closed cracks containing water is also obtained:

$$\lambda\left(P_{\mathrm{w}} - \sigma_x \sin^2\theta - \sigma_y \cos^2\theta\right)\sqrt{2\pi a} + 2\lambda P_{\mathrm{h}}\sqrt{\frac{2a}{\pi}}\arcsin\left(\frac{b}{2a}\right) + \left|\left[\left(\sigma_y - \sigma_x\right)\cos\theta\sin\theta - f\left(\sigma_x \sin^2\theta + \sigma_y\cos\theta - P_{\mathrm{w}}\right)\right]\sqrt{2\pi a}\right| = K_{\mathrm{IIc}}. \tag{12}$$

2.2. Stress Intensity Factors for Open Cracks. Unlike closed cracks, there is no friction between crack surfaces because the cracks are not closed, and there should be a curvature ρ at the crack tip. If the curvature ρ is zero, the stress singularity at the crack tip is not affected by the shear stress at the same region, which is caused by the far-field compressive stress and the flow in the crack. If the curvature ρ is not zero, the far-field compressive stress and the flow will produce a local additional stress at the crack tip. As the swelling effect, the mode I stress intensity factor induced by the additional stress acts with $K_{\mathrm{I}}^{\mathrm{p}}$ on the contrary.

The open crack is regarded as a blunt crack, and the maximum additional stress at the crack tip is equal to the compressive stress produced by the far-field compressive stress, rock swelling, and water flow:

$$\sigma_{\max} = -\left(\sigma_y - \sigma_x\right)\cos\theta\sin\theta + P_{\mathrm{h}}. \tag{13}$$

The mode I stress intensity factor $K_{\mathrm{I}}^{\mathrm{T}}$ caused by additional stress can be calculated by the following formula [33]:

$$K_{\mathrm{I}}^{\mathrm{T}} = \lim_{\rho\longrightarrow 0}\left(\frac{1}{2}\sigma_{\max}\sqrt{\rho}\right). \tag{14}$$

Then,

$$K_{\mathrm{I}}^{\mathrm{T}} = \frac{1}{2\sqrt{\pi}}\sqrt{\frac{\rho}{a}}\left[P_{\mathrm{h}} - \left(\sigma_y - \sigma_x\right)\cos\theta\sin\theta\right]\sqrt{\pi a}. \tag{15}$$

Finally, the expressions of modes I and II stress intensity factors for open crack are as follows:

$$K_{\mathrm{I}}^{\mathrm{o}} = \left(P_{\mathrm{w}} - \sigma_x \sin^2\theta - \sigma_y \cos^2\theta\right)\sqrt{2\pi a} + 2P_{\mathrm{h}}\sqrt{\frac{2a}{\pi}}\arcsin\left(\frac{b}{2a}\right) + \frac{1}{2\sqrt{\pi}}\sqrt{\frac{\rho}{a}}\left[P_{\mathrm{h}} - \left(\sigma_y - \sigma_x\right)\cos\theta\sin\theta\right]\sqrt{\pi a}, \tag{16}$$

$$K_{\mathrm{II}}^{\mathrm{o}} = \left(\sigma_x - \sigma_y\right)\cos\theta\sin\theta\sqrt{2\pi a}. \tag{17}$$

Then, the compression-shear fracture criterion for open cracks containing water is obtained:

$$\lambda\left[P_{\mathrm{w}} - \left(\sigma_x \sin^2\theta + \sigma_y \cos^2\theta\right)\right]\sqrt{2\pi a} + 2\lambda P_{\mathrm{h}}\sqrt{\frac{2a}{\pi}}\arcsin\left(\frac{b}{2a}\right) + \frac{\lambda}{2\sqrt{\pi}}\sqrt{\frac{\rho}{a}}\left[P_{\mathrm{h}} - \left(\sigma_y - \sigma_x\right)\cos\theta\sin\theta\right]\sqrt{\pi a} + \left|\left(\sigma_x - \sigma_y\right)\cos\theta\sin\theta\sqrt{2\pi a}\right| = K_{\mathrm{IIc}}. \tag{18}$$

3. Physical and Numerical Experimental Verification of Stress Intensity Factors

3.1. Verification of Physical Experiments for Open Cracks. For open cracks, a set of physical experiments were performed on rock specimens with boundary cracks in different water-bearing states to verify the accuracy of the stress intensity factors. In the experiments, red sandstone was selected as the test material, and the rock specimens were processed into the prismatic specimens with the size of 60 mm × 60 mm × 120 mm. An inclined crack was prefabricated at the top center of the specimen, with a length of 30 mm and an angle of 80° with the horizontal direction. The boundary cracks were cut with a wire saw, and the crack tip was polished with steel wire. The size of the prismatic specimen is shown in Figure 2(a).

By soaking the rock, rock specimens of four water-bearing states were prepared, which are natural, water content of 2.3%, water content of 2.5%, and natural saturation states. Compared with the weight of the dried sample, the water content of the rock is about 1.8% in the natural state and 3.3% in the natural saturated state. Four specimens were made for each water-bearing state. The uniaxial compression experiments were carried out on the MTS-816 test machine. In the tests, the compression rate was 0.002 mm/s. The specimens during the tests are shown in Figures 2(b) and 2(c).

Figure 3 shows the stress-strain relations of rocks with boundary open crack under four water-bearing conditions, where the stress and strain for each water-bearing state were averaged the experimental results in the same water-bearing states. It can be found that water intrusion greatly weakens the ultimate stress of rock. From the natural state to the saturated state, the ultimate stresses of rock for crack initiation decreased by 47.7%. The elastic modulus of rock slowly decreases with the increase of water content, indicating that the property of rock exhibits the trend from brittleness to plasticity under the action of water.

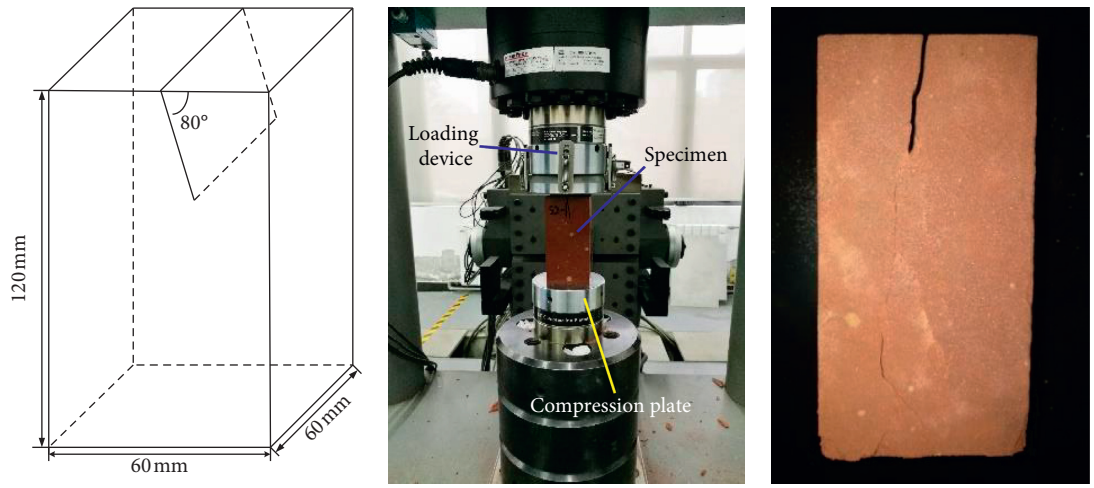

(a) (b) (c)

Figure 2: Rock specimens for uniaxial compression experiment. (a) Specimen size. (b) Before test. (c) After test.

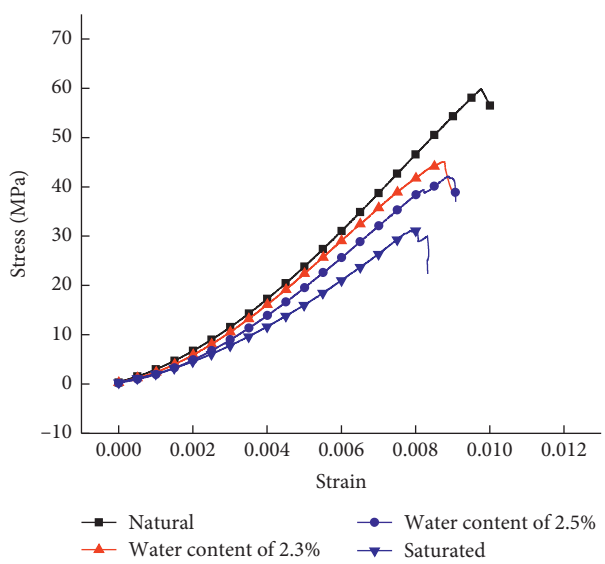

Figure 3: Stress-strain relations of rocks with open crack in different water-bearing states.

Table 1 compares the ultimate stresses obtained from the physical experiments and the theoretical values calculated by using equation (18). The ultimate stress from test for each water-bearing state was averaged the experimental results in the same water-bearing states. The relative errors are also shown in Table 1. By comparing the experimental and theoretical results, it can be seen that the relative errors are less than 5%, indicating that the calculated ultimate stresses are in good agreement with the measured ones. Furthermore, the theoretical results are usually smaller than the experimental ones of the rock. It means that the ultimate stress of rock with open crack calculated by equation (18) is conservative and has a certain safety factor.

3.2. Verification of Numerical Experiments for Closed Cracks. For closed cracks, taking account of the difficulty in processing closed cracks in physical experiments, numerical models are established by ABAQUS finite element analysis software. Figure 4 illustrates the numerical model of 120 mm height, 60 mm width, and 20 mm thickness. The crack length is 30 mm, with a horizontal angle of 80°. Eight-node hexahedral elements with reduced integration were adopted in the FEM. The size of element was 2 mm × 2 mm × 2 mm and the total number of the elements was 18000. The fixed displacement constraints were set at the bottom of the FEM model. The uniform pressure of 30 MPa was loaded on the top of the model. The models with boundary cracks are numerically analyzed by XFEM module. The crack tip element is selected as the object in the FEM analysis. Due to the existence of friction between crack surfaces during the compression-shear fracture of closed cracks, the influence of friction coefficient between crack surfaces on stress intensity factor is dominant. Consequently, the pore pressure and swelling characteristics of rocks are not considered in the present simulation for simplicity. The elastic modulus E of 800 MPa and Poisson's ratio μ of 0.25 were used in the FEM. The maximum principal stress was used as the initial damage criterion of the material, and the value was set as 25 MPa. The parameter of damage evolution was 0.0005. The viscosity coefficient of 0.1 for damage stabilization was to facilitate convergence of the results.

Table 2 compares the theoretical and numerical results, and the relative errors are also shown in the table. It is found that the relative errors of modes I and II stress intensity factors are less than 5% when the friction between closed cracks is taken into account. The theoretical calculation results of mode II stress intensity factor are in good agreement with the numerical results.

4. Analysis of Influencing Factors on Stress Intensity Factors

Whether closed cracks (equations (9) and (11)) or open cracks (equations (16) and (17)), in addition to stress conditions, the factors affecting stress intensity factors mainly

Table 1: Comparison of experimental and theoretical results of ultimate stress.

Water-bearing state	Experimental result (MPa)	Theoretical result (MPa)	Relative error (%)
Natural	59.891	58.637	2.09
Water content of 2.3%	45.071	44.257	1.81
Water content of 2.5%	41.730	40.168	3.74
Saturated	31.329	30.931	1.27

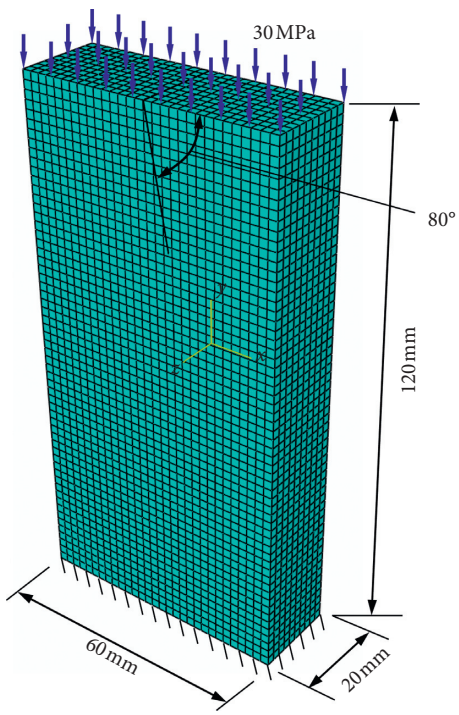

Figure 4: Numerical model with closed crack.

include crack inclination, friction coefficient of crack surface, crack length, and pore pressure in water-bearing rocks. In the following section, the sensitivity of parameters of compression-shear boundary cracks containing water under different pore pressures and lateral pressures is analyzed.

4.1. Effect of Crack Inclination on Modes I and II Stress Intensity Factors. When rock saturates naturally, the friction coefficient between crack surfaces is assumed to be 0.8. The relationship between stress intensity factor of closed crack and crack inclination is drawn as follows.

Figures 5 and 6 show the influence of crack inclination on stress intensity factors of compression-shear boundary cracks under different pore pressures. Compared with Figures 5 and 6, it can be found that the variation trend of stress intensity factor with crack inclination is basically the same under the same pore pressure, whether the crack is open or closed. When the crack inclination is constant, the stress intensity factor increases with the increase of pore pressure. According to equation (17) and Figures 5 and 6, it can be seen that the tendency of the mode I fracture of the crack becomes more obvious with the increase of the inclination angle of the crack. At the same time, the more the increase of pore pressure, the more the increase of the mode I stress intensity factor. The existence of pore pressure is also conducive to crack propagation in mode I. It shows that the contribution of water to crack propagation is mainly due to the weakening effect on the physical and mechanical properties of the rock, thus affecting the fracture toughness of the rock. Moreover, as the crack inclination increases, the mode I stress intensity factor increases gradually in a shape of "*S*." And the rate of change is faster at the beginning, then tends to be stable, and finally slows down. At the stage where the rate of change tends to be stable, the inclination varies between 25° and 65°, and the increase of stress intensity factor is more than 75%. Figures 5(b) and 6(b) show that the mode II stress intensity factor decreases first and then increases as the crack inclination increases. When the closed crack inclination is 65°, K_{II}^{b} reaches the minimum value; when the open crack inclination is 45°, $K_{\mathrm{II}}^{\mathrm{b}}$ reaches the minimum value. Due to the friction between the crack surfaces, the closed crack has a larger absolute value of the mode II stress intensity factor when the crack inclination angle is close to horizontal. For the open crack, the absolute value of the mode II stress intensity factor first increases and then decreases as the crack inclination angle increases, and it reaches the maximum at $\theta = 45°$, showing a parabolic form. This indicates that if the crack inclination angle is too large or too small, it is not conducive to the crack propagation for the open cracks. Namely, when the boundary crack is close to the boundary or perpendicular to the boundary, it is not easy to expand.

Figures 7 and 8 show the influence of crack inclination on stress intensity factors of compression-shear boundary cracks under different lateral pressures. Comparing Figure 7 with Figure 8, the mode I and II stress intensity factors of the open crack and the closed crack are almost the same as the crack inclination angle under the same lateral pressure. According to Figures 7(a) and 8(a), the influence of crack inclination on mode I stress intensity factor is suppressed as the lateral pressure increases. The variation range of mode I stress intensity factor of crack under the relatively higher lateral pressure is less than that under the relatively lower lateral pressure. When the inclination angle is less than 10°, it can be considered that the lateral pressure has no effect on $K_{\mathrm{I}}^{\mathrm{b}}$. Later, with the increase of angle, the inhibition of lateral pressure on $K_{\mathrm{I}}^{\mathrm{b}}$ becomes more and more obvious. Since the inclination of the downward crack is generally above 60°, the compression-shear crack is less prone to mode I crack propagation when the lateral pressure increases. It can be found from Figures 7(b) and 8(b) that the effect of lateral pressure on $K_{\mathrm{II}}^{\mathrm{b}}$ is consistent with that of pore pressure when the inclination of crack is constant for mode II stress intensity factor. That is, the higher the lateral pressure is, the

Table 2: Error analysis of theoretical and numerical results for closed crack.

Friction coefficient	Stress intensity factor (MPa·m$^{1/2}$)	Theoretical result	Numerical result	Relative error (%)
$f = 0$	K_{I}	−1.0774	−1.0812	0.35
	K_{II}	−2.9600	−3.0301	2.31
$f = 0.2$	K_{I}	−1.0774	−1.0369	3.91
	K_{II}	−2.7445	−2.8770	4.61
$f = 0.3$	K_{I}	−1.0774	−1.0603	1.61
	K_{II}	−2.6368	−2.5444	3.63
$f = 0.4$	K_{I}	−1.0774	−1.0546	2.16
	K_{II}	−2.5291	−2.5282	0.04
$f = 0.5$	K_{I}	−1.0774	−1.0707	0.63
	K_{II}	−2.4213	−2.4438	0.91
$f = 0.6$	K_{I}	−1.0774	−1.0369	3.91
	K_{II}	−2.3136	−2.3272	0.59
$f = 0.7$	K_{I}	−1.0774	−1.0792	0.16
	K_{II}	−2.2058	−2.1945	0.51
$f = 0.8$	K_{I}	−1.0774	−1.0650	1.15
	K_{II}	−2.0981	−2.1462	2.29

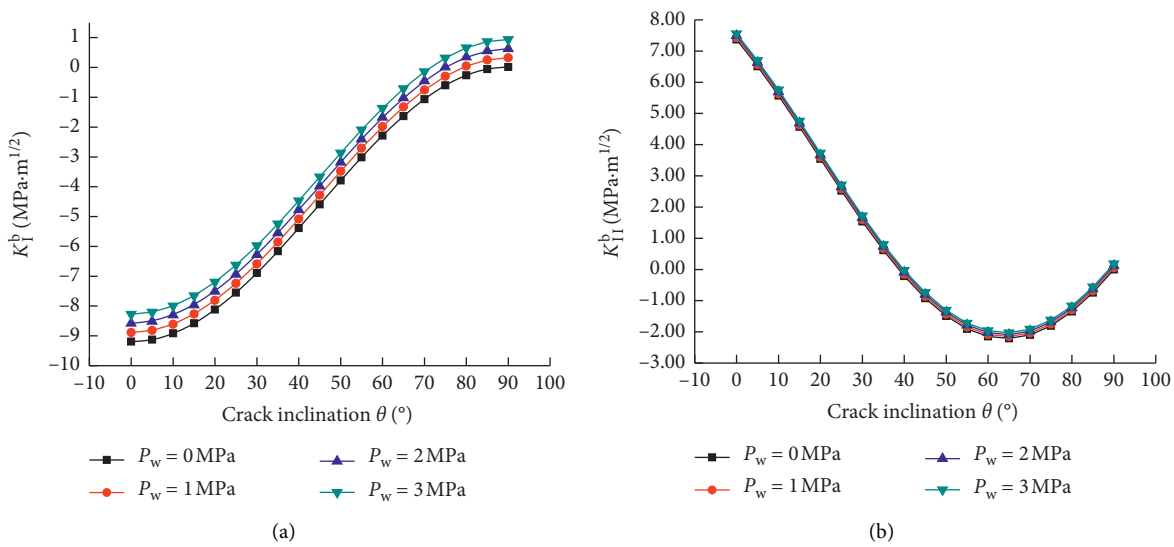

Figure 5: Relationship between crack inclination and stress intensity factor of closed cracks with different pore pressures ($f = 0.8$, $\sigma_x = 0$ MPa). (a) Mode I. (b) Mode II.

greater the stress intensity factor of mode II is. In addition, as the crack inclination angle increases, the variation range of $K_{\mathrm{II}}^{\mathrm{b}}$ at a relatively higher lateral pressure is smaller than that at a relatively lower lateral pressure. Combined with Figures 5 and 6, it is shown that the variation range of modes I and II stress intensity factor decreases significantly as the lateral pressure increases gradually, and the change of crack inclination is no longer the main factor affecting the crack growth.

4.2. Influence of Friction Coefficient of Crack Surface on Stress Intensity Factor. Figure 9 shows the relationship between mode II stress intensity factor and friction coefficient under the high ($\sigma_x = 25$ MPa) and low ($\sigma_x = 0$ MPa) lateral pressures.

The friction coefficient f between the crack surfaces mainly affects the mode II stress intensity factor $K_{\mathrm{II}}^{\mathrm{b}}$ of the closed crack. As shown in Figure 9, $K_{\mathrm{II}}^{\mathrm{b}}$ is proportional to the friction coefficient f. When the lateral pressure is very small, the mode II stress intensity factor is negative. With the increase of friction coefficient between crack surfaces, the absolute value of mode II stress intensity factor decreases, which indicates that the increase of friction coefficient is not conducive to crack growth. At this time, the larger the pore pressure is, the smaller the decline rate of $|K_{\mathrm{II}}^{\mathrm{b}}|$ is. It can be concluded that the pore pressure greatly weakens the determination of friction coefficient on mode II stress intensity factor. If the pore pressure reaches a larger value, the effect of friction coefficient on $K_{\mathrm{II}}^{\mathrm{b}}$ can be neglected, indicating that the crack is in the open state at this time, which is consistent with the actual situation. When the lateral pressure is high,

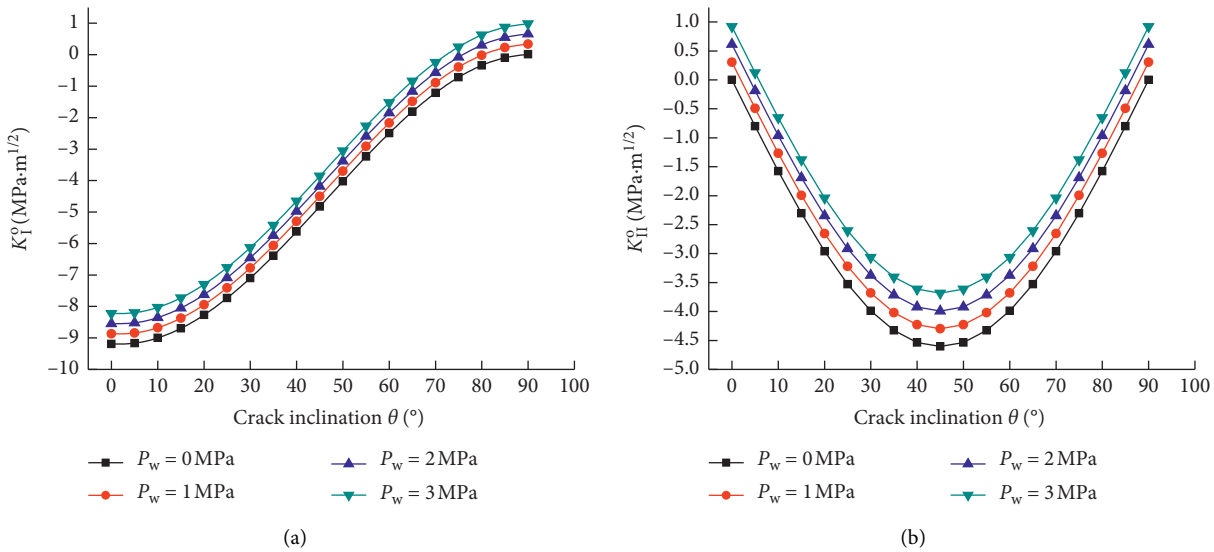

Figure 6: Relationship between crack inclination and stress intensity factor of open cracks with different pore pressures ($\sigma_x = 0$ MPa). (a) Mode I. (b) Mode II.

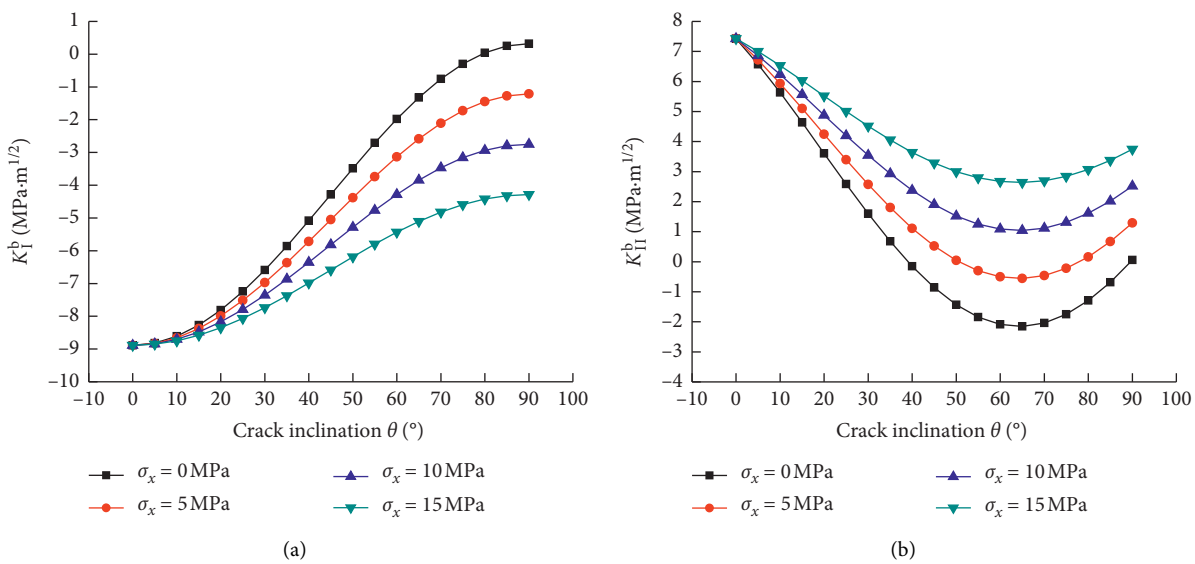

Figure 7: Relationship between crack inclination and stress intensity factor at different lateral pressures of closed crack ($f = 0.8$, $P_w = 0$ MPa). (a) Mode I. (b) Mode II.

the mode II stress intensity factor is positive. With the increase of friction coefficient, the mode II stress intensity factor and its absolute value increase. This shows that the increase of friction coefficient is beneficial to crack propagation under the high lateral pressure. The smaller the pore pressure is, the larger the growth rate of $|K_{II}^b|$ is and the smaller variation of curve slope is. This indicates that the small variation of pore pressure has little effect on the mode II stress intensity factor with friction coefficient at high lateral pressure. In addition, when $f = 0.2$, pore pressure P_w changes from 0 MPa to 3 MPa, and mode II stress intensity factor increases by 72.6% and 30.9% at the high and low lateral pressures, respectively. When $f = 0.8$, the mode II stress intensity factor increases by 3.4% and 9.4%, respectively, under the above two lateral pressures. It is shown that the greater the friction coefficient is, the smaller the effect of the pore pressure on the mode II stress intensity factor is, whether at the high lateral pressure or the low lateral pressure. On the contrary, Figure 10 shows that, considering pore pressure is constant, the greater the friction coefficient is, the greater the influence of lateral pressure on mode II stress intensity factor is.

4.3. Influence of Crack Length on Stress Intensity Factor. Figures 11 and 12 show the relationships between crack length and stress intensity factor for the closed and open cracks, respectively. It can be found that the stress

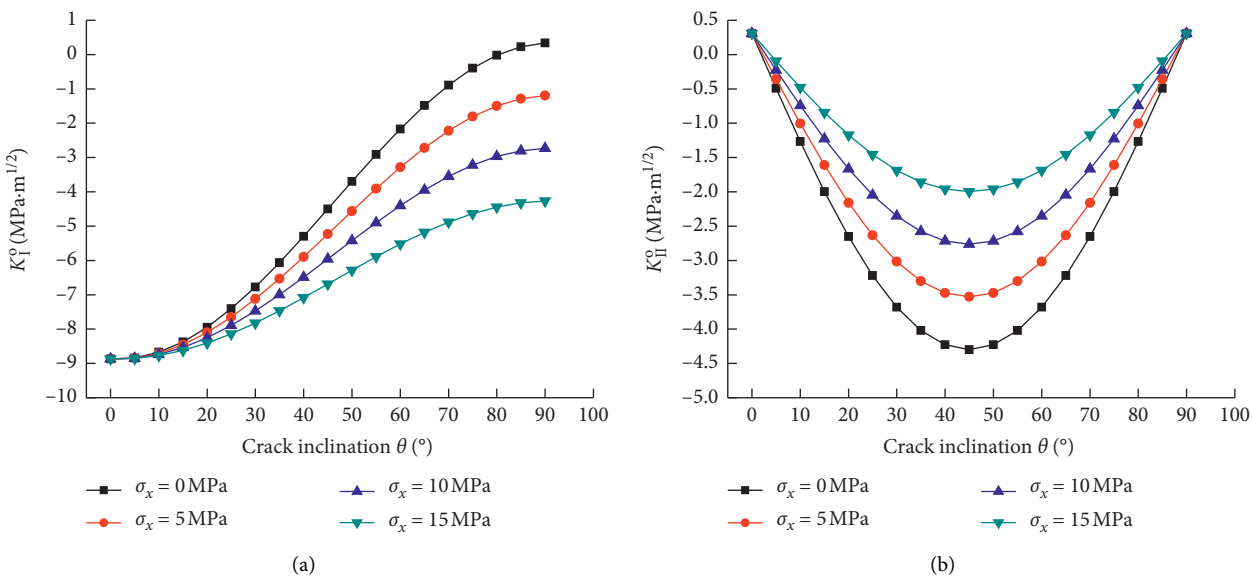

Figure 8: Relationship between crack inclination and stress intensity factor at different lateral pressures of open crack ($P_w = 0$ MPa). (a) Mode I. (b) Mode II.

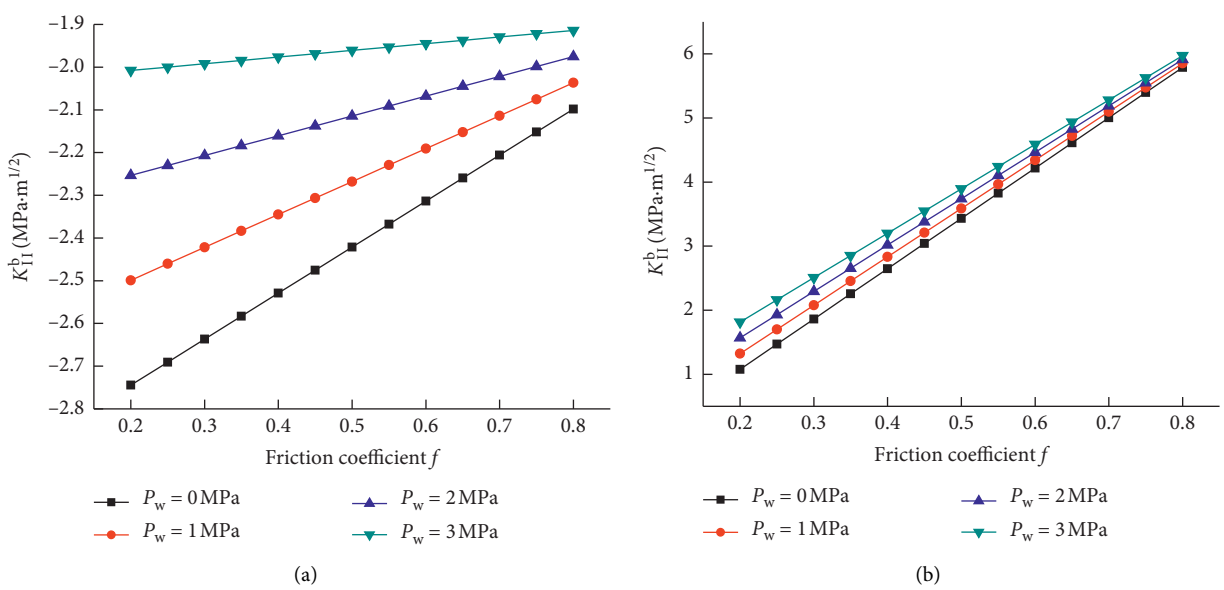

Figure 9: Relationship between mode II stress intensity factor and friction coefficient. (a) $\sigma_x = 0$ MPa. (b) $\sigma_x = 25$ MPa.

intensity factor decreases as the crack length increases, whether it is a closed crack or an open crack. For closed crack, when $a < 0.05$ m, the modes I and II stress intensity factors decrease rapidly as the crack length increases. And then, the decreasing rate of stress intensity factor decreases slowly as the crack length increases. For open cracks, as the crack length increases, the decreasing rate of stress intensity factor decreases gradually with no obvious turning point. Furthermore, the decrease range of modes I and II stress intensity factors of the two types of cracks is also very small.

4.4. Effect of Crack Inclination and Friction Coefficient on Ratio of I and II Stress Intensity Factor. The stress intensity factor of crack is the key index to influence whether crack propagates or not, but the propagating of compression-shear crack also depends on the compression-shear coefficient λ. In this section, the relationships between the critical compression-shear coefficient λ_c and the crack inclination or the friction coefficient of the crack surface are discussed.

Equations (12) and (18) show that when the critical compression-shear coefficient is used to judge whether the rock is fractured or not, the criteria for judging the fracture

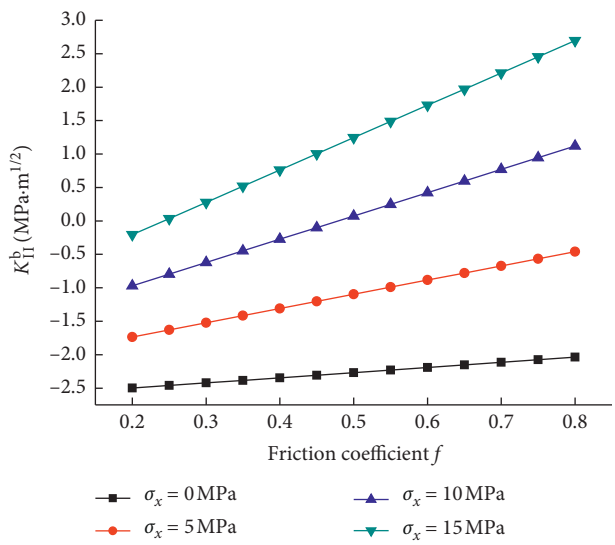

Figure 10: Relationship between friction coefficient and mode II stress intensity factor at different lateral pressure of closed cracks ($P_w = 0$ MPa).

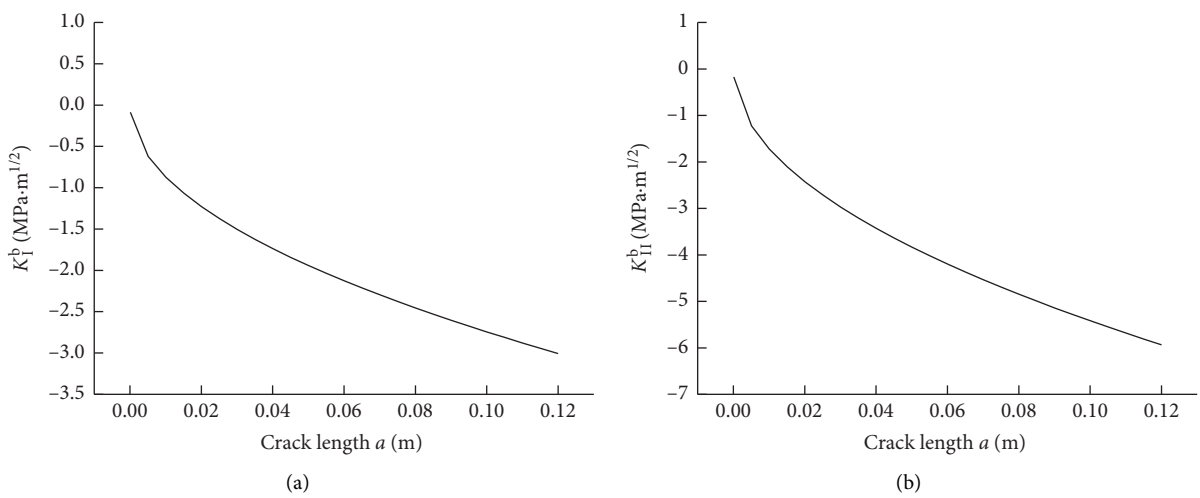

Figure 11: Relationship between closed crack length and stress intensity factor ($\theta = 70^\circ$). (a) Mode I. (b) Mode II.

are symbolically related to the mode I stress intensity factor. When $K_I < 0$, if the crack propagates, $\lambda < \lambda_c$; when $K_I > 0$, if the crack propagates, $\lambda > \lambda_c$.

Figure 13 shows the relationship between the critical compression-shear coefficient and the crack inclination of closed crack. It can be seen from Figure 13 that the critical compression-shear coefficient always changes near 0 when the crack inclination is less than 40°. At the moment, the mode I stress intensity factor is negative when the crack inclination is close to the horizontal direction. According to the aforementioned criteria, if the crack propagates in case of $K_I < 0$, then $\lambda < \lambda_c$. In fact, the compression-shear coefficient of rock is generally larger than the calculated critical value at this time, so the crack is not easy to propagate in this state. Subsequently, the growth rate of the compression-shear coefficient is accelerated until the crack inclination is 85°, where λ_c is 38. When the crack inclination is greater than 85°, the critical compression-shear coefficient λ_c decreases rapidly. When the crack inclination is 90°, the critical compression-shear coefficient decreases again to nearly 0. At this stage, mode I stress intensity factor continues to increase with the increase of crack inclination, and mode I fracture gradually becomes the main fracture mode.

Figure 14 shows the relationship between critical compression-shear coefficient and friction coefficient when the crack inclination is 70°. At this time, pore pressure and lateral pressure are both 0 MPa. It is shown that the critical compression-shear coefficient decreases with the increase of friction coefficient between crack surfaces. The value of mode I stress intensity factor is negative at this time. When the crack propagates, the compression-shear coefficient λ should be less than the critical compression-shear coefficient λ_c, that is, $\lambda < \lambda_c$. This shows that the increase of friction coefficient is not conducive to crack propagation at this moment.

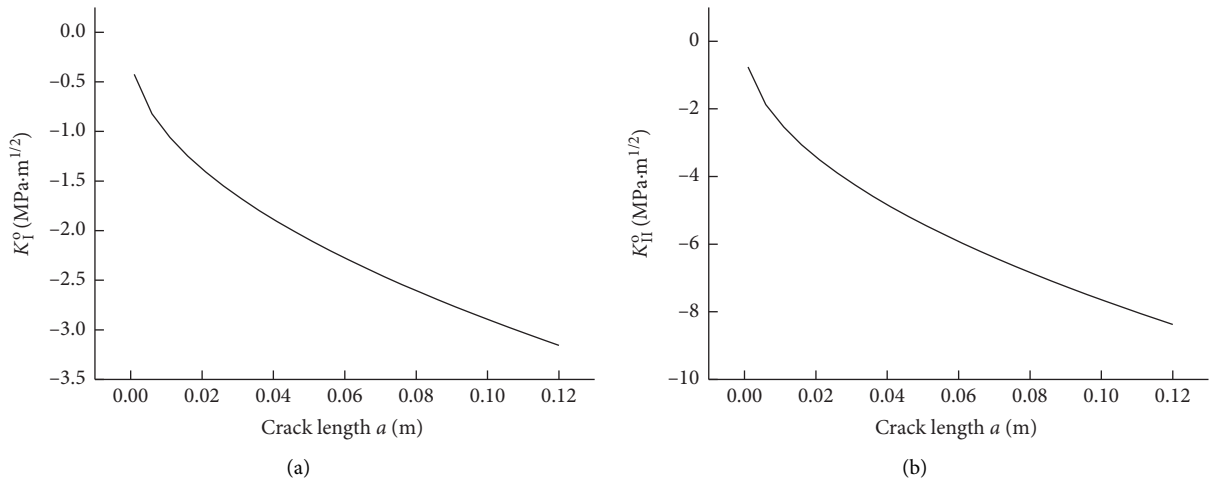

Figure 12: Relationship between open crack length and stress intensity factor ($\theta = 70^\circ$). (a) Mode I. (b) Mode II.

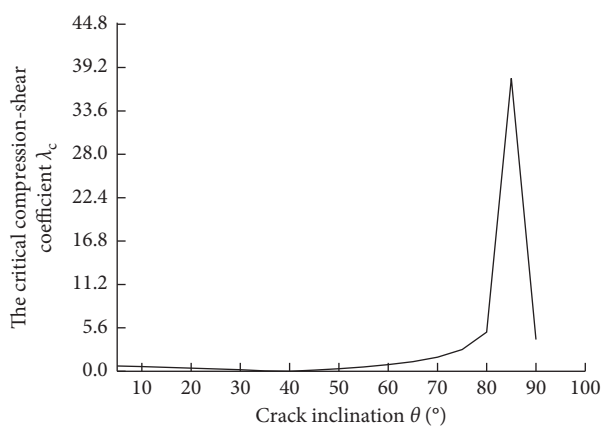

Figure 13: Relationship between critical compression-shear coefficient and crack inclination of closed crack.

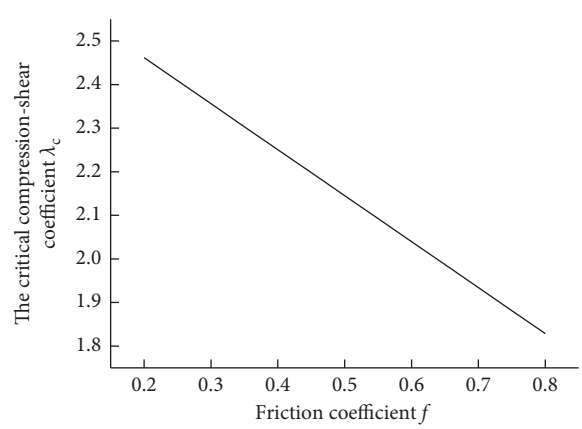

Figure 14: Relationship between critical compression-shear coefficient of closed crack and friction coefficient of crack surface ($\theta = 70^\circ$).

5. Conclusions

The fracture behavior of boundary cracks containing water in rock is discussed in this study. The detailed calculation methods of stress intensity factors for closed and open cracks are proposed by considering the influences of pore pressure, lateral pressure, friction coefficient between closed cracks, and the swelling effect.

Combining the stress intensity factors with the fracture criterion, the role of compression-shear coefficient in judging the crack initiation was highlighted. The compression-shear coefficient is related to the properties of rock materials. It can reveal the contribution of each aforementioned factor to crack initiation.

The effect of water on crack propagation is mainly due to the deterioration of the physical and mechanical properties of the rock; that is, the fracture toughness is degraded. The small range change of pore pressure has little effect on the stress intensity factor. For the closed cracks, the effect of friction coefficient on mode II stress intensity factor is inhibited by the increase of pore pressure at the relatively lower lateral pressure.

This study provides a theoretical basis for estimating the instability law of boundary cracks in rock materials by compression-shear coefficient. Further studies should be performed to apply the proposed fracture theory to rock mass or water-resisting layers.

Data Availability

The data used to support the findings of this study are available from the corresponding author upon request.

Conflicts of Interest

The authors declare that they have no conflicts of interest.

Acknowledgments

The authors acknowledge gratefully the support provided by the National Key Basic Research Program of China (2015CB251602), the National Natural Science Foundation of China (51308533), and the Postgraduate Research & Practice Program of Education & Teaching Reform of CUMT (YJSJG-2018-029).

References

[1] E. Z. Lajtai, R. H. Schmidtke, and L. P. Bielus, "The effect of water on the time-dependent deformation and fracture of a granite," *International Journal of Rock Mechanics and Mining Sciences & Geomechanics Abstracts*, vol. 24, no. 4, pp. 247–255, 1987.

[2] L. N. Y. Wong, V. Maruvanchery, and G. Liu, "Water effects on rock strength and stiffness degradation," *Acta Geotechnica*, vol. 11, no. 4, pp. 713–737, 2016.

[3] H. Masoumi, J. Horne, and W. Timms, "Establishing empirical relationships for the effects of water content on the mechanical behavior of gosford sandstone," *Rock Mechanics and Rock Engineering*, vol. 50, no. 8, pp. 2235–2242, 2017.

[4] L. Zhuang, K. Y. Kim, M. Diaz, and S. Yeom, "Evaluation of water saturation effect on mechanical properties and hydraulic fracturing behavior of granite," *International Journal of Rock Mechanics and Mining Sciences*, vol. 130, Article ID 104321, 2020.

[5] D. Ma, X. Cai, Q. Li, and H. Duan, "In-situ and numerical investigation of groundwater inrush hazard from grouted karst collapse pillar in longwall mining," *Water*, vol. 10, no. 9, p. 1187, 2018.

[6] Z. Zhou, X. Cai, D. Ma et al., "Water saturation effects on dynamic fracture behavior of sandstone," *International Journal of Rock Mechanics and Mining Sciences*, vol. 114, pp. 46–61, 2019.

[7] S.-Q. Yang, Y.-H. Huang, and P. G. Ranjith, "Failure mechanical and acoustic behavior of brine saturated-sandstone containing two pre-existing flaws under different confining pressures," *Engineering Fracture Mechanics*, vol. 193, pp. 108–121, 2018.

[8] J.-P. Zuo, M.-H. Yao, Y.-J. Li, S.-K. Zhao, Y.-Q. Jiang, and Z.-D. Li, "Investigation on fracture toughness and micro-deformation field of SCB sandstone including different inclination angles cracks," *Engineering Fracture Mechanics*, vol. 208, pp. 27–37, 2019.

[9] D. Guha Roy, T. N. Singh, J. Kodikara, and R. Das, "Effect of water saturation on the fracture and mechanical properties of sedimentary rocks," *Rock Mechanics and Rock Engineering*, vol. 50, no. 10, pp. 2585–2600, 2017.

[10] Y. Yao, "Linear elastic and cohesive fracture analysis to model hydraulic fracture in brittle and ductile rocks," *Rock Mechanics and Rock Engineering*, vol. 45, no. 3, pp. 375–387, 2012.

[11] B. Huang and J. Liu, "Experimental investigation of the effect of bedding planes on hydraulic fracturing under true triaxial stress," *Rock Mechanics and Rock Engineering*, vol. 50, no. 10, pp. 2627–2643, 2017.

[12] M. D. Kuruppu and K. P. Chong, "Fracture toughness testing of brittle materials using semi-circular bend (SCB) specimen," *Engineering Fracture Mechanics*, vol. 91, pp. 133–150, 2012.

[13] I. L. Lim, I. W. Johnston, S. K. Choi, and J. N. Boland, "Fracture testing of a soft rock with semi-circular specimens under three-point bending. Part 1—mode I," *International Journal of Rock Mechanics and Mining Sciences & Geomechanics Abstracts*, vol. 31, no. 3, pp. 185–197, 1994.

[14] I. L. Lim, I. W. Johnston, S. K. Choi, and J. N. Boland, "Fracture testing of a soft rock with semi-circular specimens under three-point bending. Part 2—mixed-mode," *International Journal of Rock Mechanics and Mining Sciences & Geomechanics Abstracts*, vol. 31, no. 3, pp. 199–212, 1994.

[15] B. Mahanta, A. Tripathy, V. Vishal, T. N. Singh, and P. G. Ranjith, "Effects of strain rate on fracture toughness and energy release rate of gas shales," *Engineering Geology*, vol. 218, pp. 39–49, 2017.

[16] M. Kataoka, Y. Obara, and M. Kuruppu, "Estimation of fracture toughness of anisotropic rocks by semi-circular bend (SCB) tests under water vapor pressure," *Rock Mechanics and Rock Engineering*, vol. 48, no. 4, pp. 1353–1367, 2015.

[17] Z. Zhou, X. Cai, D. Ma, W. Cao, L. Chen, and J. Zhou, "Effects of water content on fracture and mechanical behavior of sandstone with a low clay mineral content," *Engineering Fracture Mechanics*, vol. 193, pp. 47–65, 2018.

[18] M. Tiennot, J.-D. Mertz, and A. Bourgès, "Influence of anisotropic microcracking due to swelling on the fracture toughness of a clay-bearing sandstone," *Rock Mechanics and Rock Engineering*, vol. 50, no. 11, pp. 2861–2870, 2017.

[19] W. Hua, S. Dong, Y. Li, and Q. Wang, "Effect of cyclic wetting and drying on the pure mode II fracture toughness of sandstone," *Engineering Fracture Mechanics*, vol. 153, pp. 143–150, 2016.

[20] I. Gupta, C. Sondergeld, and C. Rai, "Fracture toughness in shales using nano-indentation," *Journal of Petroleum Science and Engineering*, vol. 191, Article ID 107222, 2020.

[21] A. A. Savitski and E. Detournay, "Propagation of a penny-shaped fluid-driven fracture in an impermeable rock: asymptotic solutions," *International Journal of Solids and Structures*, vol. 39, no. 26, pp. 6311–6337, 2002.

[22] N. Dutler, M. Nejati, B. Valley, F. Amann, and G. Molinari, "On the link between fracture toughness, tensile strength, and fracture process zone in anisotropic rocks," *Engineering Fracture Mechanics*, vol. 201, pp. 56–79, 2018.

[23] J. Wu, M. Feng, B. Yu, and G. Han, "The length of pre-existing fissures effects on the mechanical properties of cracked red sandstone and strength design in engineering," *Ultrasonics*, vol. 82, pp. 188–199, 2018.

[24] W. Dong, S. Song, B. Zhang, and D. Yang, "SIF-based fracture criterion of rock-concrete interface and its application to the prediction of cracking paths in gravity dam," *Engineering Fracture Mechanics*, vol. 221, Article ID 106686, 2019.

[25] G. C. Sih, "Strain-energy-density factor applied to mixed mode crack problems," *International Journal of Fracture*, vol. 10, no. 3, pp. 305–321, 1974.

[26] Q. L. Zhou, "Compress shear fracture criterion of rock and it's application," *Chinese Journal of Geotechnical Engineering*, vol. 9, no. 3, pp. 33–37, 1987.

[27] B. Shen and O. Stephansson, "Modification of the G-criterion for crack propagation subjected to compression," *Engineering Fracture Mechanics*, vol. 47, no. 2, pp. 177–189, 1994.

[28] M. R. Ayatollahi and M. Sistaninia, "Mode II fracture study of rocks using Brazilian disk specimens," *International Journal of Rock Mechanics and Mining Sciences*, vol. 48, no. 5, pp. 819–826, 2011.

[29] A. X. Zheng and X. Q. Luo, "Research on combined fracture criterion of rock under compression-shear stress," *Rock and Soil Mechanics*, vol. 36, no. 7, pp. 1892–1898, 2015.

[30] E. David and R. W. Zimmerman, "Sliding crack model for the uniaxial compression of rock," in *Rock Mechanics: Meeting Society's Challenges and Demands*, E. Eberhardt, D. Stead, and T. Morrison, Eds., vol. 1, pp. 575–580, Taylor & Francis Group, London, UK, 2007.

[31] N. Hasebe and S. Inohara, "Stress analysis of a semi-infinite plate with an oblique edge crack," *Ingenieur-Archiv*, vol. 49, no. 1, pp. 51–62, 1980.

[32] L. Liang, J. Xiong, and X. Liu, "Experimental study on crack propagation in shale formations considering hydration and

wettability," *Journal of Natural Gas Science and Engineering*, vol. 23, pp. 492–499, 2015.

[33] J. Tirosh and E. Catz, "Mixed-mode fracture angle and fracture locus of materials subjected to compressive loading," *Engineering Fracture Mechanics*, vol. 14, no. 1, pp. 27–38, 1981.